ON THE EFFECT OF CORNER CURVATURE IN LAMINAR FLOW THROUGH A CROSS-SLOT CHANNEL

Gerardo N. Rocha
gerardorocha@portugalmail.pt
Departamento de Engenheria Electromecânica, Unidade Materiais Têxteis e Papeleiros,
Universidade da Beira Interior, Edifício das Engenharias, 6201-001, Covilhã – Portugal
Robert J. Poole
robpoole@liverpool.ac.uk
Department of Engineering, University of Liverpool, Liverpool, L69 3GH, UK
Manuel M. Alves
mmalves@fe.up.pt
Faculdade de Engenharia da Universidade do Porto, Dep.^{to} de Engenharia Química, CEFT
Rua Dr. Roberto Frias, 4200-130, Porto – Portugal
Paulo J. Oliveira
pjpo@ubi.pt
Departamento de Engenharia Electromecânica, Unidade Materiais Têxteis e Papeleiros,
Universidade da Beira Interior, Edifício das Engenharias, 6201-001, Covilhã – Portugal

Abstract. *The flow of viscoelastic liquids through a cross-slot geometry is studied by means of numerical simulations. The geometry is planar and the constitutive model follows the FENE-CR (constant shear viscosity) equation, valid for relative dilute solutions of polymeric fluids, under fully developed flow conditions. A fully implicit finite-volume numerical method is used to solve the governing equations. For Deborah numbers above a critical value (dependent on the extensibility parameter of the model L^2 and the solvent viscosity ratio β) the flow becomes asymmetric but remains steady. This effect is solely due to the elastic nature of the flowing fluid, i.e. the instability is purely elastic in nature. The main objectives of the present study are: to examine the possible effects of rounding the corners of the geometry (curvature radius of R = 0.05d and 0.5d, where d is the channels' width) for a range of values of the controlling non-dimensional parameters (De, L^2 and β); to calculate the critical Deborah number of the symmetry-breaking bifurcation; and to document on the flow asymmetries occurring in this kind of geometry. Our results are in qualitative agreement with recent experimental observations presented by Arratia et al. (2006) and numerical results for infinite extensibility models (UCM and Oldroyd-B) previously published by Poole et al. (2007).*

Keywords: *Purely elastic instabilities; Rounded corners; Viscoelastic fluid; FENE-CR model; Finite-volume method.*

1. INTRODUCTION

The application of numerical codes for the solution of fluid mechanics problems, in what is known as Computational Fluid Dynamics – CFD (Patankar, 1980; Ferziger and Peric, 2002), has seen a significant growth and has been extended to include the simulation of viscoelastic flow problems. Fluids that cannot be described by the Newtonian constitutive equation are called non-Newtonian fluids. Further, viscoelastic fluids possess elastic properties as well as viscous properties and mathematical models for this type of fluids are constantly being developed and tested in an attempt to improve the modelling process for these fluids.

Recently, there has been renewed interest to analyze the behavior of extensional flows of dilute polymer solutions through a cross-slot geometry. Our motivation was stimulated by the recent studies of viscoelastic flows through cross-slot geometry conducted by Arratia et al. (2006) and Poole et al. (2007). First, Arratia et al. (2006) have reported two novel flow instabilities of a planar extensional flow of a dilute flexible polymer solution (200 ppm of PAA to a viscous Newtonian solvent with 97%-glycerol aqueous solution) under steady forcing. They found two distinct flow instabilities at low Reynolds numbers ($Re<10^{-2}$). The first instability leads to spatial symmetry breaking and bistability, while the second produces temporal fluctuations in the velocity field. The velocity vanishes at the stagnation point at the center of the cross-slot, where the strain rate is highest and the fluid is most strongly stretched. Later, Poole et al. (2007) simulated the flow in a complete cross-slot geometry using the simplest differential viscoelastic model, the upper-convected Maxwell (UCM) model in the absence of inertia effects ($Re = 0$). Their numerical prediction results were in qualitative agreement with the experimental observations of Arratia et al. (2006). For a Newtonian fluid and low Deborah numbers ($De < 0.3$) the flow is perfectly symmetric and steady, but for Deborah numbers above a critical value ($De \approx 0.31$) the flow becomes increasingly asymmetric but remains steady. The numerical results of Poole et al. (2007) have demonstrated that a flow asymmetry, due solely to elastic effects (elasticity), can be numerically predicted in a perfectly symmetric cross-slot geometry. Finally, they concluded that the asymmetry is a consequence of the compressive nature of the flow upstream of the central-square, coupled with streamline curvature, rather than the large elongational stresses that also appears in the flow downstream of the central-square.

The purpose of the present work is to analyze in more detail the purely elastic flow instabilities occurring in a planar cross-slot using a more realistic FENE-type model to represent the viscoelastic liquid (Bird et al., 1987), in the absence of inertial forces ($Re = 0$). Pure stretching is produced at opposing jets, such as when channels are arranged as the four "arms" of a cross. In our numerical study the fluid enters from the left and right "arms" and leaves from the top and bottom arms, and consequently a stagnation point occurs at the center where the flow is extensional (see Fig. 2(a)). To describe the rheology of the fluid we use the constant viscosity FENE-CR constitutive model proposed by Chilcott and Rallison (1988) in which the polymer architecture is modeled as a pair of beads connected by a finitely extensible nonlinear spring with a maximum extensibility of L^2. In the limit when the extensibility parameter goes to infinity ($L^2 \rightarrow \infty$) the model reduces to the well-known upper-convected Maxwell (UCM) or Oldroyd-B models which were applied in the numerical work of Poole et al. (2007). In particular, we investigate the laminar flow in a cross-slot arrangement having both sharp and rounded corners (corner radius R) for variation of elasticity (De), extensibility parameter (L^2) and solvent viscosity ratio (β). The results were obtained by application of the numerical simulation program (written in the Fortran language) developed by Oliveira et al. (1998), based on a multidimensional finite-volume formulation.

2. GOVERNING EQUATIONS

In this section, the basic conservation equations for two-dimensional (2D), incompressible and isothermal, laminar flows are presented as well as the constitutive FENE-CR model (Chilcott and Rallison, 1988). The conservation equations of mass and linear momentum in the absence of body forces are expressed by:

$$\nabla \bullet \boldsymbol{u} = 0 \tag{1}$$

and

$$\rho \frac{D\boldsymbol{u}}{Dt} = -\nabla p + \nabla \bullet \boldsymbol{\tau}_{tot} \tag{2}$$

where $\boldsymbol{u}$ is the local velocity vector (with components u and v along to the Cartesian coordinates x and y), t the time, ρ the fluid density (assumed constant), p the pressure, $D/Dt = \partial/\partial t + \boldsymbol{u} \bullet \nabla$ the substantial derivative and $\boldsymbol{\tau}_{tot}$ is the total extra stress tensor given by an appropriate constitutive equation. For a homogeneous solution of a Newtonian solvent and an additional elastic constituent (the polymeric solute), the extra stress tensor in Eq. (2) can be written as the sum of two terms: $\boldsymbol{\tau}_{tot} = \boldsymbol{\tau}_s + \boldsymbol{\tau}$. The term $\boldsymbol{\tau}$ represents the contribution from the polymer molecules, while the term $\boldsymbol{\tau}_s$ is the contribution from the solvent which follows the Newtonian constitutive equation:

$$\boldsymbol{\tau}_s = \eta_s \left(\nabla \boldsymbol{u} + \nabla \boldsymbol{u}^{\mathrm{T}} \right) \equiv 2\eta_s \boldsymbol{D} \tag{3}$$

As constitutive equation for the extra stress we employ the FENE-CR model (Chilcott and Rallison, 1988) in which the polymer molecule is modeled by two beads connected by a nonlinear spring. In this case we have:

$$\boldsymbol{\tau} + \left(\frac{\lambda}{f(\tau)} \overset{\nabla}{\boldsymbol{\tau}} \right) = 2\eta_p \boldsymbol{D} \tag{4}$$

with the extensibility function $f(\boldsymbol{\tau})$ expressed by:

$$f(\tau) = \frac{L^2 + \left(\lambda / \eta_p \right) tr(\boldsymbol{\tau})}{L^2 - 3} \tag{5}$$

In the above equations, the Oldroyd upper convected derivative is given by:

$$\overset{\nabla}{\boldsymbol{\tau}} \equiv \frac{\partial \tau}{\partial t} + \nabla \bullet \boldsymbol{u}\boldsymbol{\tau} - \nabla \boldsymbol{u}^{\mathrm{T}} \bullet \boldsymbol{\tau} - \boldsymbol{\tau} \bullet \nabla \boldsymbol{u} \tag{6}$$

and the rate of strain tensor is denoted:

$$\boldsymbol{D} = \frac{1}{2}\left(\nabla \boldsymbol{u} + \nabla \boldsymbol{u}^{\mathrm{T}}\right) \tag{7}$$

where η_s is the solvent viscosity (constant), η_p the contribution of polymer to the total shear viscosity $\eta_0 = \eta_s + \eta_p$ (also taken as constant), λ the constant zero-shear rate relaxation time, and L^2 the extensibility parameter that measures the size of the polymer molecule in relation to its equilibrium size.

There are five non-dimensional parameters to this flow problem: the radius of curvature R (geometric parameter); the solvent viscosity ratio $\beta = \eta_s / \eta_0$ (concentration parameter); the Reynolds number $Re = \rho U d / \eta_0$ (dynamic parameter); and the extensibility parameter of the FENE-CR model, L^2 , and the Deborah number, $De = \lambda U / d$ (constitutive parameters).

3. NUMERICAL METODOLOGY

Equations (1)-(5) are solved with a finite-volume CFD code developed by Oliveira et al. (1998), based on a general non-orthogonal coordinate system and the collocated mesh arrangement (see Fig. 1(a)). In this method all variables are calculated and stored at the centre of each control volume (cells), as represented schematically in Fig. 1(b).

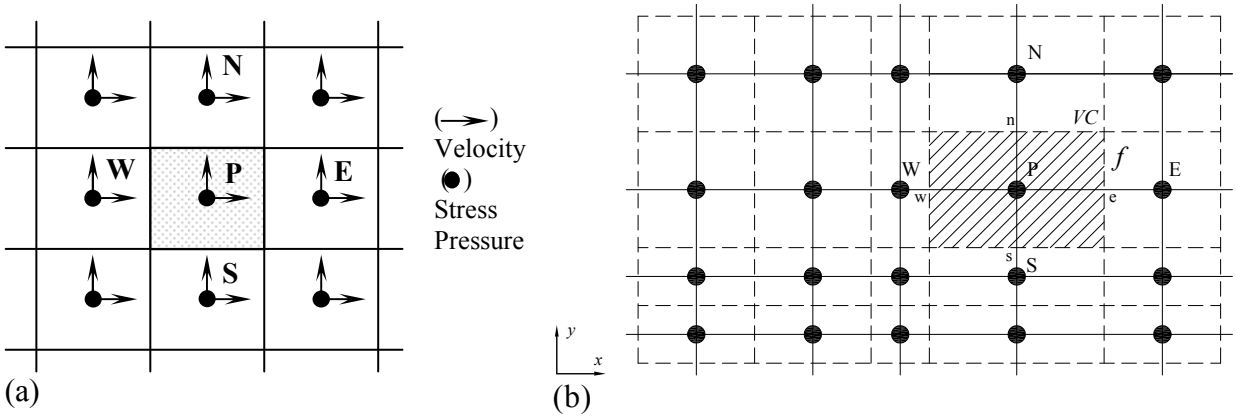

Figure 1- (a) Non-staggered mesh arrangement with all variables stored at the centre of cells. (b) Main control volume in a non-uniform mesh.

The governing equations are discretised by integration in space over control volumes (with volume V_P) and in time over time steps (denoted by Δt) using a fully implicit discretization. This process results in systems of linearised algebraic equations. The algorithm is explained with more detail in Oliveira et al. (1998) and only an outline is given in this section. The discretised constitutive FENE-CR equation at cell P is given by:

$$a_P^{\tau} \boldsymbol{\tau}_P^{(\mathrm{n}+1)} = \sum_F a_F^{\tau} \boldsymbol{\tau}_F^{(\mathrm{n}+1)} + \left\{ S_{\tau}\left(\boldsymbol{\tau}^{(n)}, \nabla \boldsymbol{u}^{(n)}\right) + S_{\tau}^{HRS}\left(\boldsymbol{\tau}^{(n)}\right) + \frac{\lambda V_P}{f\left(\tau_P\right)\Delta t} \boldsymbol{\tau}_P^{(\mathrm{n})} \right\} \tag{8}$$

with central coefficient: $a_P^{\tau} = V_P + \sum_F a_F^{\tau} + \dfrac{\lambda V_P}{f\left(\tau_P\right)\Delta t}$

where V_P is the volume of cell P and the stress coefficients a_F^{τ} are composed by convective fluxes. These convective fluxes are calculated at cell faces located between cell P and any of its neighbouring cells F (in this work the summations are over 4 neighbouring cells for W, E, S and N with compass notation: West, East, South and North, see Fig. 1(b)). The stress sources terms S_{τ} depend simultaneously on the stress tensor $\boldsymbol{\tau}$ and velocity gradients $\nabla \boldsymbol{u}$ which are evaluated at the previous time level (n).

In the first step of the algorithm the above set of linear equations (Eq. (8)), for the stress tensor, are solved sequentially by a bi-conjugate gradient method, to obtain each stress component τ_{ij} at the new time level $(n+1)$. A solution for a steady-state problem is effectively approached by a succession of time advancement steps where Δt acts as an inertial-relaxation term.

In the second step, the discretised momentum conservation equations is solved implicitly for the intermediate velocity $\boldsymbol{u}^*$:

$$a_P \boldsymbol{u}_P^* = \sum_F a_F \boldsymbol{u}_F^* + \left\{ S_u\left(\nabla p^{(n)}\right) + S_u\left(\nabla \bullet \boldsymbol{\tau}^{(n+1)}\right) + S_{u\_Dif}\left(\boldsymbol{u}\right) + S_u^{HRS}\left(\boldsymbol{u}\right) + \frac{\rho V_P}{\Delta t}\boldsymbol{u}_P^n \right\} \tag{9}$$

with: $a_P = \sum_F a_F + \dfrac{\rho V_P}{\Delta t}$

where the coefficients a_F have convective and diffusive contributions. The velocity source terms S_u (on the right hand side of Eq. (9) inside curled brackets) represent the effects due to the pressure gradient, the elastic stress divergence term, the artificial diffusive term (explicit part) and the high-resolution scheme, respectively. The last term inside the curled brackets is the inertial term resulting from the temporal derivative. All the coefficients of the discretised equations are calculated using the upwind scheme for the convective terms, and the high-resolution convective scheme CUBISTA (Alves et al., 2003) is implemented with the deferred correction technique (Khosla and Rubin, 1974) through the source terms S^{HRS}.

After updating the stress fields in the first step of the algorithm, the discretised momentum conservation equations (Eq. (9)) are solved sequentially, with the same solution method, for each velocity component (u and v). Pressure is assumed from the previous time step. In general, the velocity components $\boldsymbol{u}^*$ from solution of Eq. (9) do not satisfy the discretised continuity conservation equation, expressed by:

$$\nabla \bullet \boldsymbol{u}^{(n+1)} = 0 \tag{10}$$

The third step of the algorithm involves a correction to $\boldsymbol{u}^*$ obtained from a re-arrangement of the continuity equation into a Poisson pressure-correction equation, having the form:

$$a_P^p p'_P = \sum_F a_F^p p'_F - \left(\nabla \bullet \boldsymbol{u}^*\right) \tag{11}$$

with: $a_P^p = \sum_F a_F^p$

Equation (11) is solved implicitly solved for the pressure correction p' ($p^{(n+1)} \equiv p^* - p'$) with a matrix solver based on a symmetric conjugate gradient method. This pressure correction p' is then added to the pressure from the previous time step and is also used to correct the velocity in order to satisfy the continuity equation (Eq. (10)).

These three steps, corresponding to a time advancement from level (n) to level $(n+1)$, are repeated until the fields $\boldsymbol{\tau}^{(n+1)}$, $\boldsymbol{u}^{(n+1)}$ and $p^{(n+1)}$ remain unchanged; we say that the procedure has then "converged" (with a relative tolerance of 10^{-4}).

4. PROBLEM DESCRIPTION AND COMPUTATIONAL MESH

The flow geometry is represented in Fig. 2, where some of relevant variables are sketched. We consider the full planar cross-slot geometry. Flow enters from left and right "arms" and leaves from top and bottom "arms". All channels have a constant width of d and the inlet and outlet "arms" are ten channel widths (d) in length. The upstream and downstream lengths of the domain were sufficiently long to avoid effects of non-fully developed inlet conditions on the flow in the central square and ensure a fully developed outlet profile.

In order to test if rounding corners would significantly affect the asymmetry of the flow, we applied two geometries with rounded-corners R/d = 0.05 and 0.5 (see Fig. 2(b)) and generated meshes having the same characteristics as the sharp-corner ones, to be discussed below.

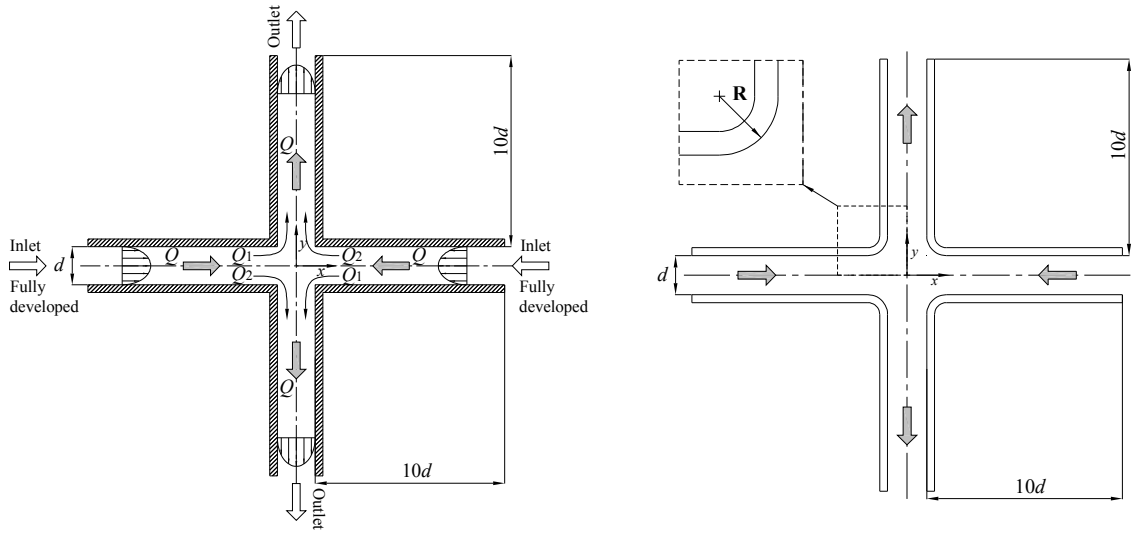

Figure 2- (a) Sketch of the cross-slot configuration and (b) solution domain for the rounded-corner geometry.

All the calculations were carried out for Re = 0 which was imposed in the computational code by equating the convective terms of the momentum equation to zero. The flow instability is purely elastic in nature and we do not want to consider inertial effects here.

In terms of mesh resolution, the geometry was divided into five blocks, as represented in Fig. 3(a), which were then used to generate the computational mesh; the numbers of cells in each block are presented in Table 1.

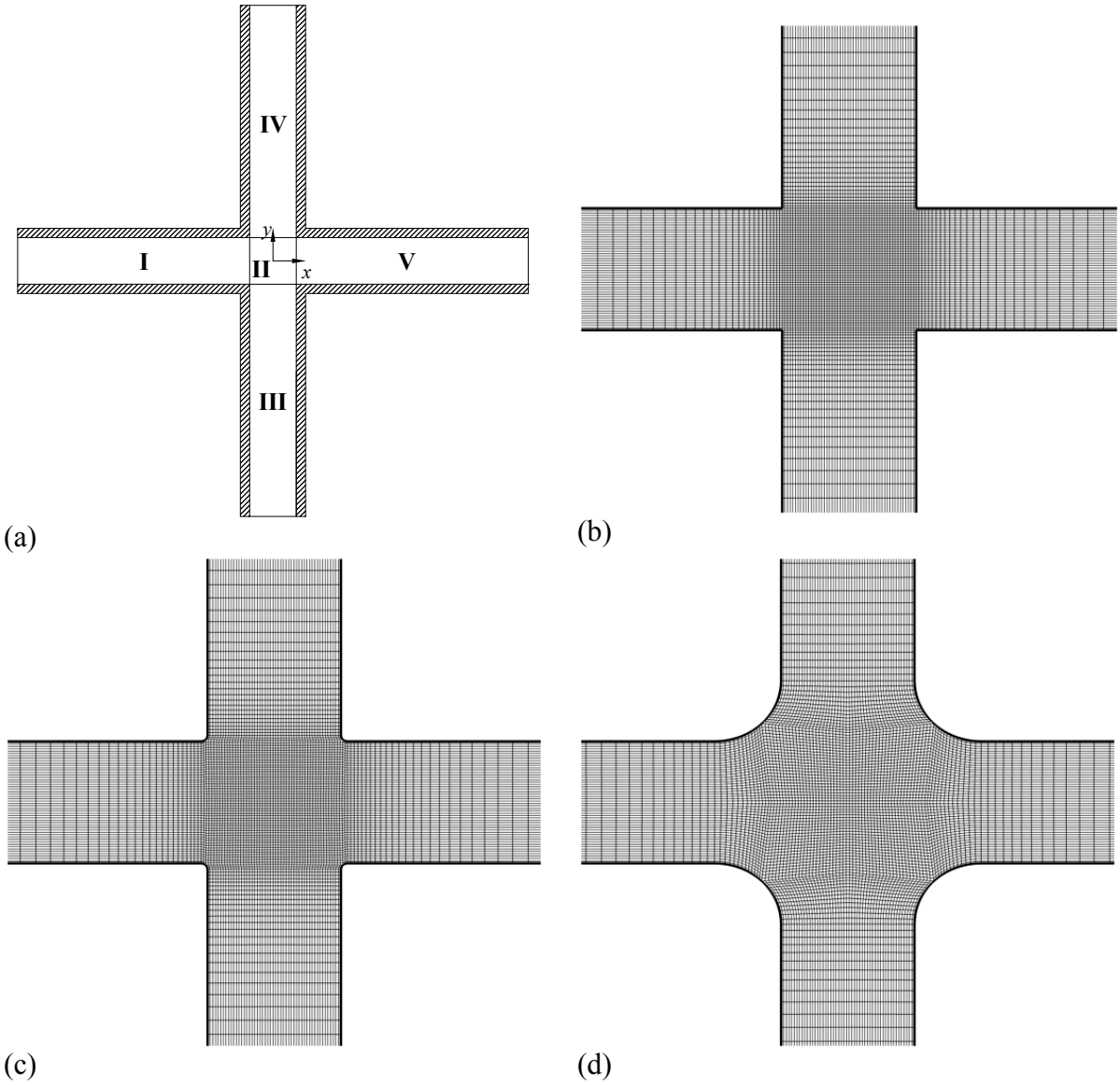

Figure 3- (a) Schematic definition of the blocks used to generate the mesh. Zoomed view ($x \in [-2d, +2d]$ and $y \in [-2d, +2d]$) of mesh for (b) sharp-corner (R = 0) and rounded corners with (c) R = 0.05d (small curvature) and (d) R = 0.5d (large curvature).

Table 1. Main characteristics of computational mesh

Blocks	N_x	N_y	f_x	f_y
I	50	51	0.929296	1.000000
II	51	51	1.000000	1.000000
III	51	50	1.000000	0.929296
IV	51	50	1.000000	1.075369
V	50	51	1.075369	1.000000
NC = 12801				

As seen in Fig. 3, the mesh is orthogonal but non-uniform along the inlet and outlet channels, with increasing concentration of cells on approaching the central square (see Fig. 3(b)-(d)). The central square ($|x|$ and $|y| \leq 0.5d$) was mapped with a uniform mesh having

cell spacing $\Delta x_{\min} \approx \Delta y_{\min} \approx 0.02d$ (block II in Fig. 3(a)). This two-dimensional mesh has a total of 12801 cells which corresponds to 76806 degrees-of-freedom. The mesh data in Table 1 include the total number of control volumes (NC), the number of cells along the x- (N_x) and y-directions (N_y), and the expansion or compression (f_x or f_y) geometrical factors in both directions. The following boundary conditions were applied:

(i) Inlet ($x = \pm 10.5d$): fully developed velocity (with average value U) and stress profiles were imposed from analytical equations;

(ii) Outlet ($y = \pm 10.5d$): Neumann conditions for all dependent variables, except the pressure which was linearly extrapolated;

(iii) Solid walls ($x = y = \pm 0.5d$): no-slip boundary conditions with stresses from analytical solutions.

All the calculations were performed with a Pentium Core 2/2.40GHz computer with 3.37GB RAM.

5. NUMERICAL RESULTS AND DISCUSSION

The main objective is to assess the effect of rounding the corners of the cross-slot geometry (R/d = 0, 0.05 and 0.5) and the results are presented in the following sequence: in subsection 5.1 we analyze the influence of elasticity by varying the Deborah number, at fixed values of $L^2 = 100$ and $\beta = 0.1$; in subsection 5.2 we analyze the influence of solvent viscosity ratio, for $\beta = 0.05$, 0.1 and 0.2, at a fixed value of $L^2 = 100$; and in subsection 5.3 we study the influence of the extensibility parameter of the FENE-CR fluid, for $L^2 = 50$, 100 and 200, at a fixed value of $\beta = 0.1$.

In this study, quantitative results are provided in terms of a bifurcation parameter DQ that quantifies the degree of asymmetry of the flow, identical to the one proposed in the work of Poole et al. (2007): $DQ = (Q_2 - Q_1)/Q$, with flow rates Q_1 and Q_2 as indicated in Fig. 2(a). The total flow rate supplied to each incoming channel is $Q = Ud$ and this incoming flow splits at the cross-slot region such that $Q = Q_1 + Q_2$. For a symmetric flow $Q_1 = Q_2$ giving $DQ = 0$, and for an asymmetric flow $Q_1 \neq Q_2$ giving $DQ \neq 0$ ($DQ = \pm 1$ for a completely asymmetric flow). Two steady solutions are then possible: a bifurcated solution with more flow coming from the left and going through the lower channel (e.g. Fig. 5(c)); and the opposite situation with more flow from the left into the upper channel.

5.1 Influence of elasticity (*De*)

As already mentioned, the Deborah number ($De = \lambda U / d$) is used to measure the influence of elasticity and represents the ratio of the relaxation time of the fluid and the characteristic time scale of the flow. Here, De was varied by varying the relaxation time parameter λ (since we assumed $d = U = 1$).

Figure 4 shows the predicted results of the degree of asymmetry (DQ) when the Deborah number was varied from 0.0 (Newtonian fluid) to 1.0, at fixed values of $L^2 = 100$ and $\beta = 0.1$, for sharp-corner (R/d = 0 – see Fig. 3(b)) and the two rounded-corners cases (R/d = 0.05 and 0.5, see Fig. 3(c) and (d), respectively).

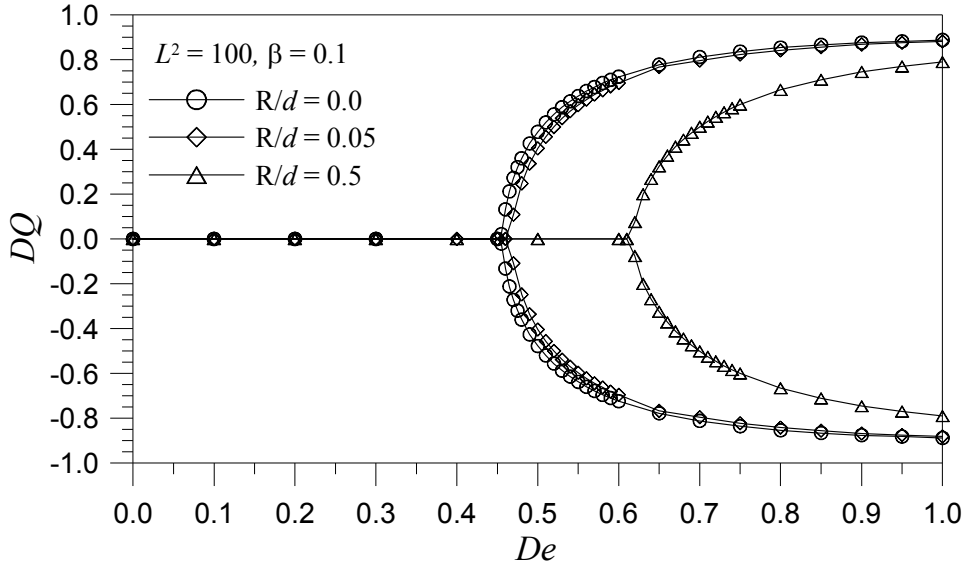

Figure 4- Effect of rounding corners (R/d = 0.0, 0.05 and 0.5) with variation of asymmetry parameter DQ vs. De, for L^2 = 100 and β = 0.1.

The results presented in Fig. 4 show transition from a symmetric to a asymmetric state when De goes above a critical Deborah number (De_{cr}). It is also clear from the results of Fig. 4 by comparing the case R = 0 with R/d = 0.05 (slightly rounded case), that both the critical Deborah number (De_{cr}) and the variation of the degree of asymmetry (DQ) are approximately the same (R/d = 0.0 → $De_{cr} \approx 0.46$ and R/d = 0.05 → $De_{cr} \approx 0.47$, see Fig. 5(c) and (g), respectively). However, when the corners are markedly rounded, as seen by the comparison against the case having R/d = 0.5 (large curvature case), the flow instability is delayed to higher values of Deborah number and $De_{cr} \approx 0.62$ (see Fig. 5(k)).

In Fig. 5 we present the predicted streamline plots for increasing, and equivalent, values of Deborah number for the three values of corner curvature R/d.

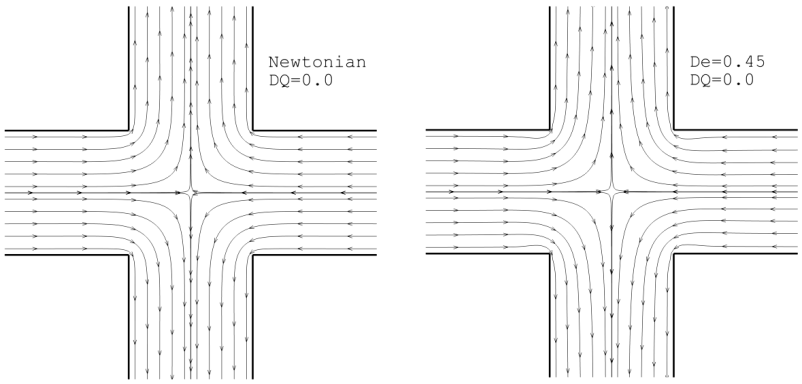

(a) (b)

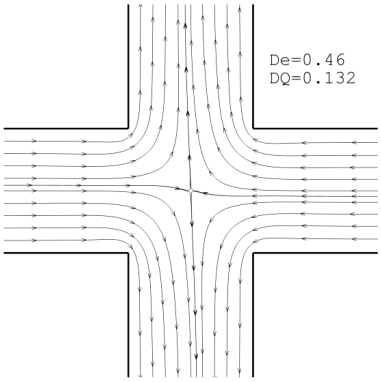
De=0.46
DQ=0.132

(c)

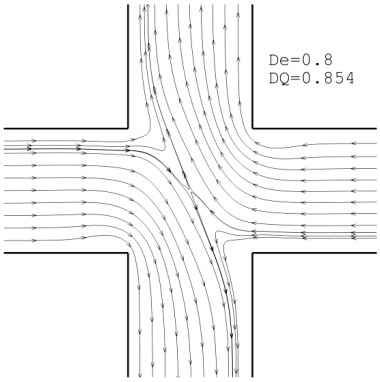
De=0.8
DQ=0.854

(d)

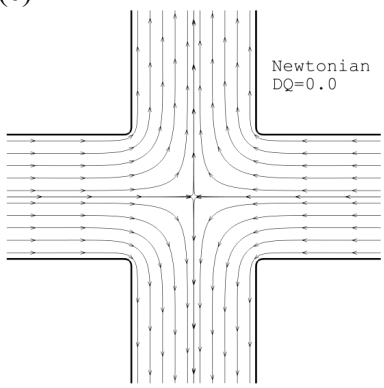
Newtonian
DQ=0.0

(e)

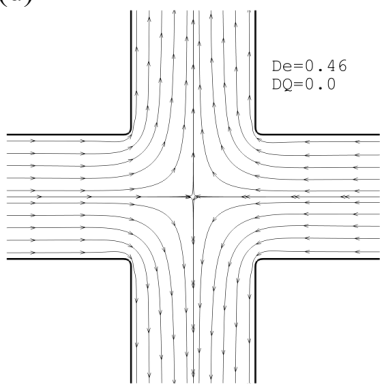
De=0.46
DQ=0.0

(f)

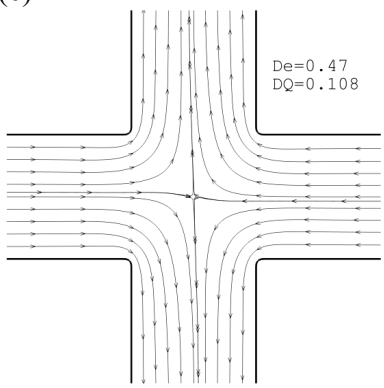
De=0.47
DQ=0.108

(g)

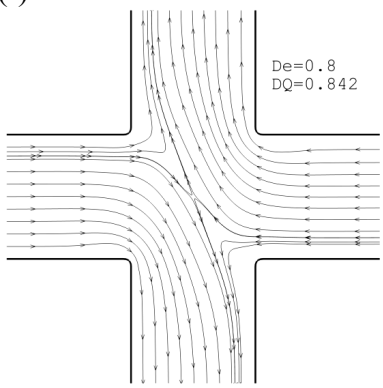
De=0.8
DQ=0.842

(h)

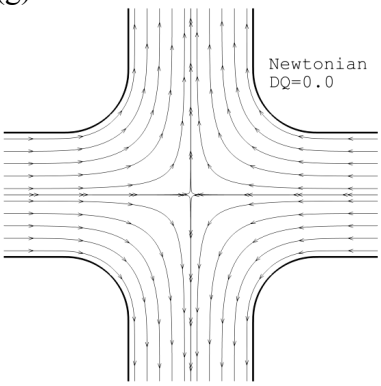
Newtonian
DQ=0.0

(i)

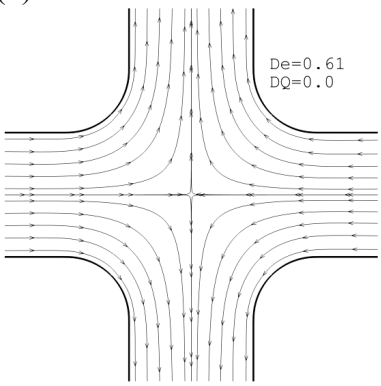
De=0.61
DQ=0.0

(j)

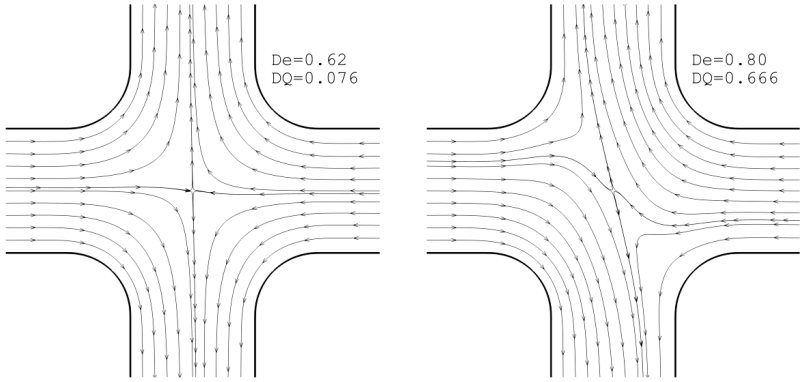

(k) (l)

Figure 5- Predicted streamline plots for: (a)-(d) sharp-corners R/d = 0.0; (e)-(h) rounded corner R/d = 0.05; and (i)-(l) rounded corner R/d = 0.5 (L^2 = 100 and β = 0.1).

As a consequence of the delay of the instability amongst the three curvature cases the velocity field is significantly altered (see Fig. 6(b)), with an anticipated reduction of the strain rate ($\dot{\varepsilon} = \partial u/\partial x$) along the centerline of the channels, on approaching and leaving the internal stagnation point at the cross-slot centre, as shown in Fig. 6(a). The corresponding maximum Newtonian strain rate, at the stagnation point, is provided in Table 2 ($\dot{\varepsilon}$ is normalized with U/d).

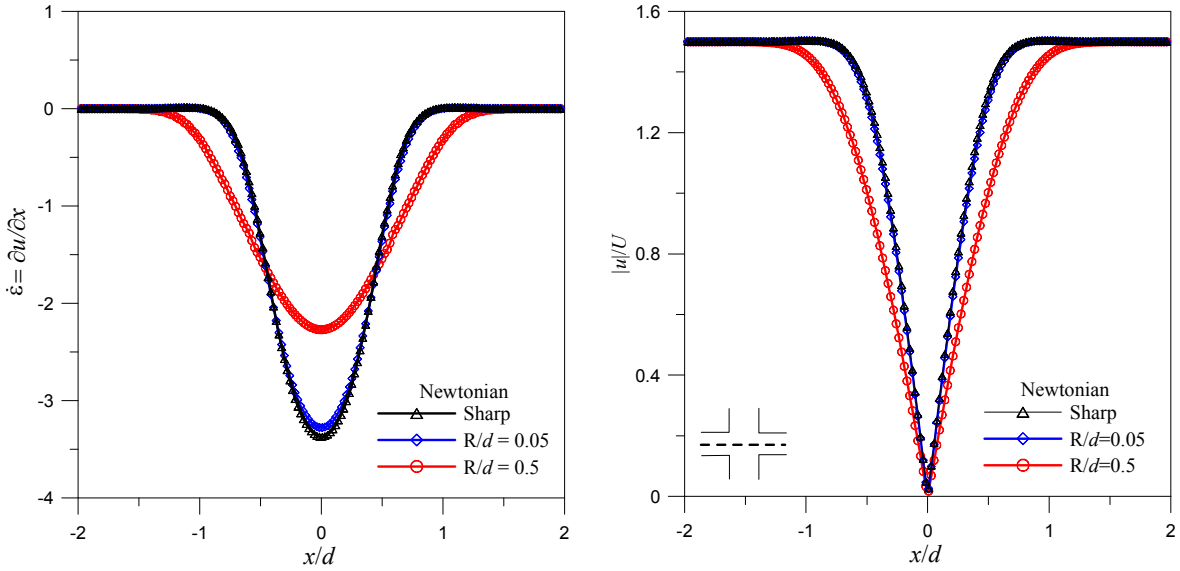

(a) (b)

Figure 6- Influence of corner curvature R/d = 0 (sharp), 0.05 and 0.5 for a Newtonian flow along the inlet centerline channels for: (a) Strain rate profiles ($\dot{\varepsilon} = \partial u/\partial x$); and (b) Velocity profiles.

Table 2. Newtonian strain rate at the stagnation point

Geometry	$\dot{\varepsilon}$
Sharp-corner	-3.346
R/d =0.05	-3.255
R/d =0.5	-2.261

We can conclude from Fig. 6 that when the corner is first only slightly rounded (R/d = 0.05) the results remain unchanged compared with the sharp-corner case, showing a strain rate difference at the stagnation point of 2.7%. However, comparing the sharp-corner case with the larger curvature case (R/d = 0.5) we see that the difference is more significative, with a strain rate difference at the stagnation point of 32%.

5.2 Influence of solvent concentration (β)

In this subsection we look at the effect of rounding the corners when varying the solvent concentration β = 0.05, 0.10 and 0.20, at a fixed L^2 = 100. The influence of solvent viscosity ratio is controlled by the β parameter which measures the ratio of Newtonian solvent shear viscosity to the total shear viscosity of the polymer solution. In other words, this parameter provides a measure of polymer concentration and by decreasing β the elasticity of the fluid becomes more dominant. The variation of the degree of asymmetry (DQ) versus the Deborah number (De) is illustrated in Fig. 7. It is observed, from the results for the sharp-corner case, for example, that an increase of the β parameter leads to a delay of the critical bifurcation point. It can be also observed, for the same β parameter, that the effect of rounding corners yields a significant change to the critical bifurcation point once R is large.

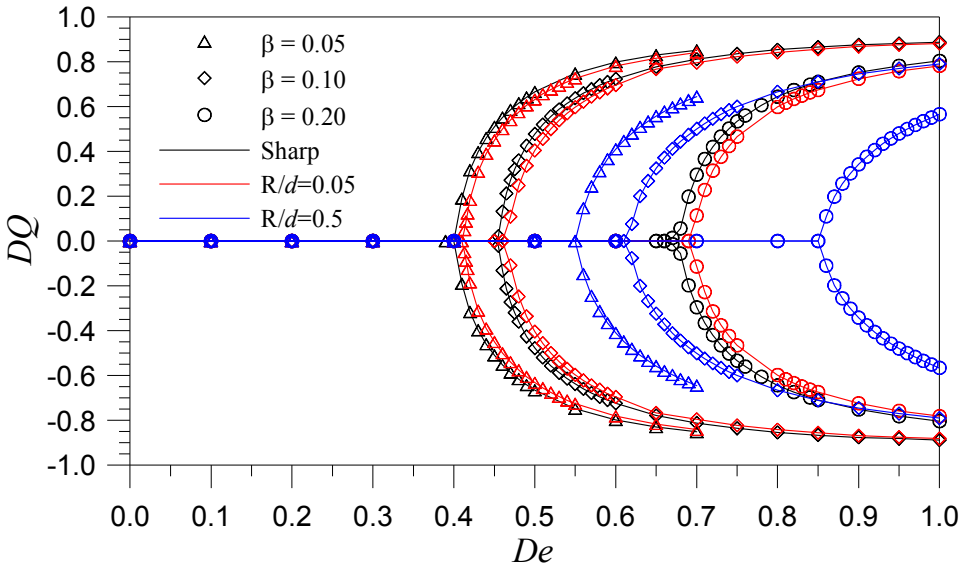

Figure 7- Effect of rounding corners (R/d = 0.0, 0.05 and 0.5) on the variation of the asymmetry parameter, DQ vs. De, for several solvent viscosity ratios (L^2 = 100).

Quantitative results of the critical Deborah number (De_{cr}) for each β parameter, showing the effect of rounding corners, are given in Table 3. As can be seen, the critical Deborah number (at fixed L^2 = 100) depends both on the value of β and on the degree of corner curvature, once R becomes significant. As mentioned above, by increasing the value of the β parameter, we delay the bifurcation flow instability and therefore this parameter controls the point of transition between symmetric and asymmetric flow (see for example the case of sharp-corners).

Table 3. Computed values of the critical Deborah number (De_{cr}) for selected values of the solvent viscosity β and L^2=100.

β	Sharp-corner	R/d = 0.05	R/d = 0.5
0.05	0.41	0.42	0.56
0.10	0.46	0.47	0.62
0.20	0.68	0.70	0.86

5.3 Influence of extensibility parameter (L^2)

This parameter measures the extensional characteristics of the fluid and represents the square of the ratio between the maximum and the equilibrium lengths of the polymer molecules. The results show that an increase of L^2 tends to accentuate the bifurcation phenomenon, that is the base flow becomes less stable, and tends to shift the occurrence of the transition point to asymmetry to lower Deborah numbers. The extensibility was seen to have a strong effect and for example, for L^2 = 50 the flow was symmetric up to $De_{cr} \approx 0.61$, but if L^2 was increased to 200 the asymmetry appears at $De_{cr} \approx 0.41$.

Results of the influence of the extensibility parameter, in terms of the variation of the asymmetry degree (DQ) vs. Deborah number (De), are given graphically in Fig. 8 and the corresponding critical Deborah numbers for each case are listed in Table 4. With the highly rounded geometry and the smaller extensibility parameter, the critical Deborah number has shifted to higher values (more than doubling the smallest De_{cr}) and the asymmetry is markedly reduced.

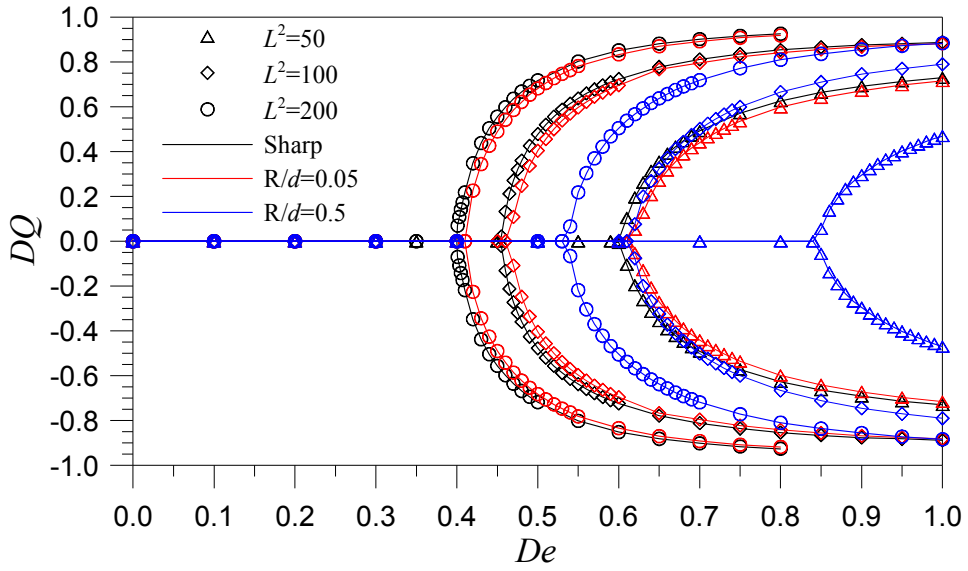

Figure 8- Effect of rounding corners (R/d = 0.0, 0.05 and 0.5) on the variation of the asymmetry parameter, DQ vs. De, for several extensibility parameters L^2 (β = 0.1).

Table 4. Computed values of the critical Deborah number (De_{cr}) for selected values of the extensibility parameter L^2 and β=0.1.

L^2	Sharp-corner	R/d = 0.05	R/d = 0.5
50	0.61	0.63	0.85
100	0.46	0.47	0.62
200	0.41	0.42	0.54

6. CONCLUSIONS

Numerical simulations of the flow of a FENE-CR model fluid through a planar cross-slot geometry have been presented in the absence of inertia effects ($Re = 0$). Steady-state results were carried out in a range of $De = 0 - 1$ for the full domain geometry, and the effect of rounding corners was studied in conjunction with the influence of elasticity (controlled by Deborah number), of the solvent concentration (controlled by β parameter) and, finally, of the extensibility parameter (controlled by L^2 parameter). It is shown that the triggering mechanism for the bifurcation phenomenon is not controlled by slightly rounding of the corners, since the extensional strain rate at the cross-slot center is not affected by such small level of wall curvature. The elasticity directly drives the instability of the flow and a De_{cr} defines the transition point from symmetric to asymmetric flow. For De values lower than De_{cr} the flow is symmetric and stable, while for values above De_{cr} the flow becomes asymmetric and the DQ parameter grows for increasing De. The solvent viscosity ratio β which is a measure of the polymer concentration (polymer concentration $c \propto 1/\beta$), when reduced, leads to an anticipation of the bifurcation phenomenon (see Fig. 7). Finally, the extensibility parameter L^2, which controls the extensional viscosity of the fluid, has a strong effect in the flow and for increasing L^2 the critical point controlled by the Deborah number decreases substantially (see Fig. 8).

Acknowledgements

The authors would like to acknowledge the financial support from Fundação para a Ciência e a Tecnologia (FCT, Portugal) under grant SFRH/BD/22644/2005 (G.N. Rocha) and projects PTDC/EME-MFE/70186/2006 and PTDC/EQU-FTT/1800/2006.

REFERENCES

Alves, M. A., Oliveira, P. J., & Pinho, F. T., 2003. A convergent and universally bounded interpolation scheme for the treatment of advection. *Int. J. Numer. Mech. Fluids*, vol. 41, pp. 47-75.

Arratia, P. E., Thomas, C. C., Diorio, J. D., & Gollub, J. P., 2006. Elastic instabilities of polymer solutions in extensional flows. *Physical Review Letters*, vol. 96, n. 14, pp. 144502.

Bird, R. B., Curtiss, C. F., Armstrong, R. C., & Hassager, O., 1987. *Dynamics of Polymeric Liquids: Kinetic Theory*. John-Wiley & Sons.

Chilcott, M. D., & Rallison, J. M., 1988. Creeping flow of dilute polymer solutions past cylinders and spheres. *J. Non-Newtonian Fluid Mech.*, vol. 29, pp. 381-432.

Ferziger, J. H., & Peric, M., 2002. *Computational Methods for Fluid Dynamics*. Springer-Verlag.

Khosla, P. K., & Rubin, S. G., 1974. A diagonally dominant second-order accurate implicit scheme. *Computers and Fluids*, vol. 2, pp. 207-209.

Oliveira, P. J., Pinho, F. T., & Pinto, G. A., 1998. Numerical simulation of non-linear elastic flows with a general collocated finite-volume method. *J. Non-Newtonian Fluid Mech.*, vol. 79, pp. 1-43.

Patankar, S. V., 1980. *Numerical Heat Transfer and Fluid Flow*. Hemisphere Publishing Corporation.

Poole, R. J., Alves, M. A., & Oliveira, P. J., 2007. Purely-elastic flow asymmetries. *Physical Review Letters*, vol. 99, n. 16, pp. 164503.